



CHORUS

This is the accepted manuscript made available via CHORUS. The article has been published as:

New cubic carbon phase via graphitic sheet rumpling

Jian-Tao Wang, Changfeng Chen, and Yoshiyuki Kawazoe

Phys. Rev. B **85**, 214104 — Published 5 June 2012

DOI: [10.1103/PhysRevB.85.214104](https://doi.org/10.1103/PhysRevB.85.214104)

New Cubic Carbon Phase via Graphitic Sheet Rumpling

Jian-Tao Wang,^{1,2,*} Changfeng Chen,² and Yoshiyuki Kawazoe³

¹*Beijing National Laboratory for Condensed Matter Physics,*

Institute of Physics, Chinese Academy of Sciences, Beijing 100190, China

²*Department of Physics and High Pressure Science and Engineering Center,*

University of Nevada, Las Vegas, Nevada 89154, USA

³*Institute for Materials Research, Tohoku University, Sendai, 980-8577, Japan*

We identify by *ab initio* calculations a new cubic carbon phase in $Pa\bar{3}$ (T_h^6) symmetry, which has a unit cell that comprises eight sp^3 -connected C_3 triangle rings (thus termed cubic C_3). The transformation from graphite occurs via a novel sheet-rumpling mechanism under anisotropic compression along the $a[100]$ axis, which is distinct from the usual c -axis compression mechanism for the graphite-to-diamond transition. Calculated structural parameters and simulated x-ray diffraction of cubic C_3 match the experimental data, thus resolving the long-standing problem of structural determination of a new carbon phase [Science **140**, 817 (1963)]. The sheet-rumpling pathway unveiled here establishes a new mechanism for structural transformation in layered covalent materials.

PACS numbers: 61.50.Ks, 61.66.Bi, 62.50.-p, 63.20.D-

Phase transformation of graphite is among the most intriguing topics in materials science. Graphite transforms into hexagonal and cubic diamond under high-pressure (above ~ 13 GPa) and high-temperature (above ~ 1300 K) conditions;¹⁻⁵ however, the transition mechanism remained unclear for decades after the synthesis of diamond from graphite. The key breakthrough comes from the study of an unquenchable transparent and hard phase that has long been observed during the cold-compression (at room temperature) stage⁶⁻¹² and is characterized by a marked increase in electrical resistivity⁷⁻¹⁰ above 15 GPa. Recent experimental and computational efforts finally identified two structural forms for cold-compressed graphite, a monoclinic M carbon¹³ and an orthorhombic W carbon,¹⁴ which provide the critical link bridging the graphite-to-diamond phase transformation.¹⁵ Another long-standing problem in graphite-originated phase transformation concerns an enigmatic cubic carbon phase discovered five decades ago.¹⁶ The experiment first observed a similar sharp rise in resistance at 15 GPa and then recorded an additional structural transformation above 50 GPa to a new phase. X-ray diffraction (XRD) indexed the new carbon phase as cubic with a unit cell edge of 5.45 Å containing 24 atoms; its structure is consistent with the space groups $Pm\bar{3}m$, $P432$, $P43m$, $Pm\bar{3}$, $P4_232$, $Pa\bar{3}$, or possibly $P23$ or $P2_13$.¹⁶ Similar structure was later observed in heated soot¹⁷ and thin films of carbon formed by chemical vapor deposition (CVD).¹⁸ Despite extensive past efforts, the structure of this new carbon phase and the atomistic mechanism for its transformation from graphite remain unresolved.

In this Brief Report, we carried out an extensive structural search, using *ab initio* calculations, through the P -type cubic structure from the low space group $P23$ (no. 195) toward the high space group $Pn\bar{3}m$ (no. 224). Besides the so-called "cubic graphite" C_6 carbon in $Pn\bar{3}m$ symmetry and $B_{12}N_{12}$ fullerene-like C_4 carbon in $Pm\bar{3}m$ (no. 221) symmetry, we here have identified a new cubic phase in $Pa\bar{3}$ (no. 205) symmetry, which is a three-

dimensional sp^3 -connected network of trigonal C_3 rings (termed cubic C_3 carbon hereafter). Its simulated XRD pattern and lattice parameter best match the experimental data.^{16,17} Moreover, we unveil a new synthesis route via a graphitic sheet rumpling and twisting process under anisotropic compression along the $a[100]$ direction of graphite.

The calculations were carried out using the density functional theory as implemented in the Vienna *ab initio* simulation package (VASP).¹⁹ Both local density approximation (LDA) in the form of Ceperley-Alder²⁰ and generalized gradient approximation (GGA) developed by Perdew, Burke and Ernzerhof (PBE)²¹ were adopted for the exchange-correlation potential. The all-electron projector augmented wave (PAW) method²² was adopted with $2s^22p^2$ treated as valence electrons. A plane-wave basis set with an energy cutoff of 800 eV was used and gave well converged total energy of ~ 1 meV per atom. The energy minimization is done over the atomic and electronic degrees of freedom using the conjugate gradient iterative technique with a $6\times 6\times 6$ k -mesh in the Brillouin zone. Band structures are calculated using the hybrid functionals (HSE06)²³ under LDA and GGA. Phonon dispersion curves are calculated using the package MedeA²⁴ with the forces calculated from VASP.

We first characterize the structural, electronic and mechanical properties of the new cubic C_3 carbon phase. There are eight C_3 triangles [Fig. 1(a)] and four zigzag C_6 benzene rings [Fig. 3(d)] in the unit cell. At zero pressure, the equilibrium lattice parameter is $a = 5.309$ Å with only one inequivalent crystallographic site, occupying the 24d (0.437, 0.340, 0.204) position. The C-C bond lengths are 1.523 and 1.525 Å for the trigonal C_3 rings and zigzag C_6 rings, respectively. These values are larger than 1.42 Å for C-C bonds in graphite, but they are almost equal to the value of 1.53 Å in diamond. Meanwhile, there are two different bond angles, 60° and 102.89° in the trigonal C_3 rings and zigzag C_6 rings, respectively. The value of 60° is much less than that in

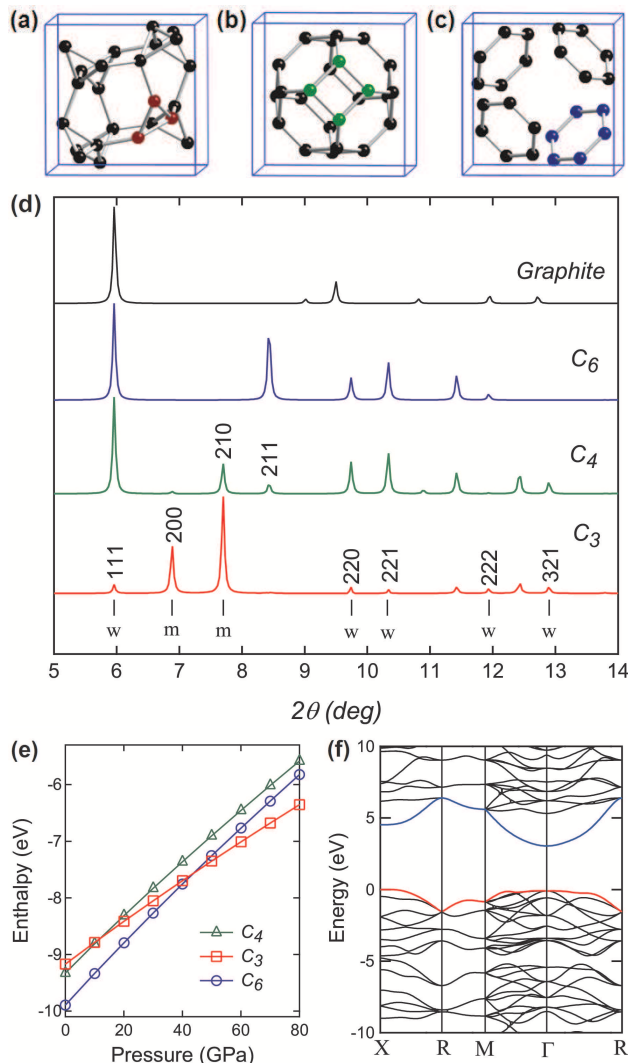


FIG. 1: (color online). (a) New cubic C₃ phase in $Pa\bar{3}$ (T_h^6) symmetry; (b) Cubic C₄ in $Pm\bar{3}m$ (O_h^1) symmetry;²⁶ (c) Cubic C₆ in $Pn\bar{3}m$ (O_h^4) symmetry.²⁹ (d) XRD patterns for cubic C₃, C₄, C₆, and hexagonal graphite. The lattice parameters for three cubic carbon structures are set to the experimental data 5.545 Å.¹⁶ X-ray wavelength is 0.3329 Å. The experimental XRD patterns and intensities¹⁶ are indicated by short lines, *w* (weak) or *m* (medium). (e) Enthalpies versus pressure for cubic C₃, C₄ and C₆ carbon. (f) Calculated electronic band structure of C₃ carbon at 0 GPa. The valence band top and the conduction band bottom are at the X and Γ point, respectively.

diamond (109.47°), implying a strained state in C₃ carbon compared to diamond. Nevertheless, the new phase is relatively stable at atmospheric pressure, as heating in a vacuum at 450°C for 6 hours.¹⁶ By fitting the calculated total energy as a function of volume to the third-order Birch-Murnaghan equation, we obtain the bulk modulus (B_0) of cubic C₃ carbon as 342 GPa, which is ~ 26% smaller than that for diamond (466 GPa).

We performed a systematic structural analysis within

TABLE I: Calculated equilibrium lattice parameter (a in Å), volume (V in Å³/atom), density (ρ in g/cm³), and band gap (E_g in eV) for diamond, cubic C₃, C₄, and C₆ carbon phase at zero pressure, compared to available experimental data³⁰ for diamond and the new cubic phase.^{16,17}

Structure	Method	a (Å)	V (Å ³)	ρ (g/cm ³)	E_g (eV)
Diamond	LDA	3.534	5.516	3.61	5.43
	GGA	3.569	5.683	3.51	5.27
	Exp. ³⁰	3.567	5.673	3.52	5.47
C ₆ -224	LDA	6.032	9.145	2.18	3.75
	GGA	6.094	9.430	2.11	3.72
	LDA ²⁹	6.033	9.149	2.19	
C ₄ -221	LDA	5.865	8.407	2.37	2.92
	GGA	5.919	8.641	2.31	3.04
	GGA ²⁶	5.933	8.702	2.29	
C ₃ -205	LDA	5.309	6.223	3.19	3.05
	GGA	5.366	6.438	3.09	2.96
	Exp. ¹⁶	5.545	7.104	2.81	
	Exp. ¹⁷	5.450	6.745	2.96	

the symmetry constraints imposed by the experimental structural parameters and XRD results^{16,17}. Our results conclusively exclude two previously proposed candidate phases, a B₁₂N₁₂ fullerene-like structure consisting of six four-membered rings [Fig. 1(b)]^{25–27} and a simple cubic C₂₄ carbon phase, the so-called "cubic graphite", consisting of four six-membered benzene rings [Fig. 1(c)].^{27–29} The simulated XRD patterns of cubic C₃, C₄, C₆, and hexagonal graphite are presented in Fig. 1(d) and compared against the experimental XRD results.¹⁶ Several major discrepancies with experimental results rule out cubic C₄ and C₆ phases: (1) both phases show a strong (111) peak at 6.0°, which reflects the sp^2 bonding environment that closely resembles that in graphite, but it is in sharp contrast to the weak peak observed in experiment; (2) both phases lack the (200) peak at 6.9° that shows stronger (medium) intensity in the experimental XRD; (3) Cubic C₆ has no (210) peak while C₄ has a relatively weak (210) peak, which is inconsistent with the relatively stronger (medium) (210) peak observed in experiment; (4) both C₄ and C₆ phases show a (211) peak but none was seen in experiment. Meanwhile, the simulated XRD patterns for cubic C₃ carbon match well with these major features and most other minor ones in the experimental XRD.¹⁶

Figure 1(e) show the calculated enthalpy as a function of pressure for C₃, C₄ and C₆ carbon. We can see that the so-called "cubic graphite" is favorable at low pressure, and C₃ carbon is more favorable at high pressure, while C₄ is unfavorable throughout the pressure range.³¹ These results further support the structural assignment of cubic C₃ for the new cubic carbon phase under high pressure.

Considering the very small samples obtained in experiment and the relatively low conversion of the new phase found from powdered graphite under high pressures,¹⁶ we

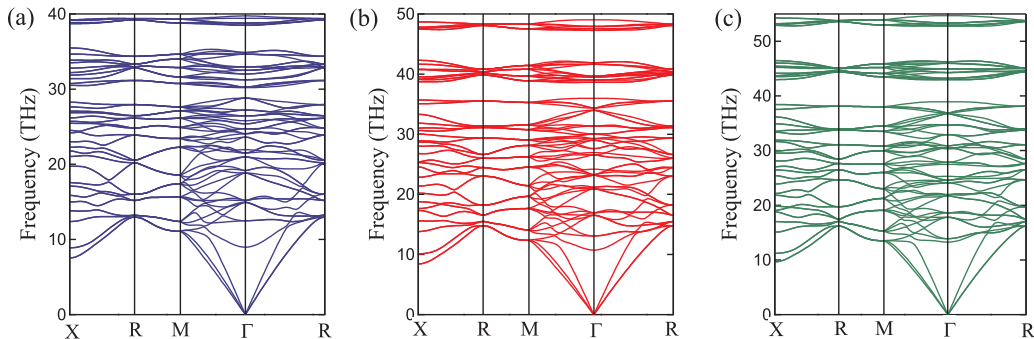


FIG. 2: (color online). Calculated phonon dispersion curves of C_3 carbon at (a) 0 GPa, (b) 80 GPa, and (c) 160 GPa.

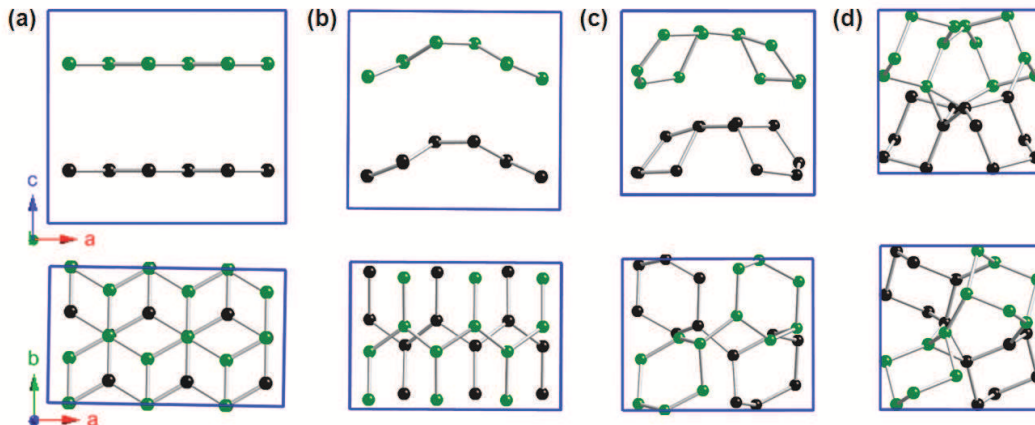


FIG. 3: (color online). The wave-like rumpling phase conversion process from graphite toward cubic C_3 phase at 60 GPa. Side (up) and top (down) views: (a) graphite in AB stacking shown in a rectangular supercell in $P6_3/mmc$ (no.194) symmetry; (b) structure at step 12 along the pathway with a wave-like rumpling carbon sheet in $Pbcn$ (no.60) symmetry; (c) structure at step 21 with a local rotation of benzene rings in $Pbca$ (no.61) symmetry; (d) the final cubic C_3 carbon showing four distorted benzene rings in $Pa\bar{3}$ (no.205) symmetry with a site shift of $(\frac{1}{4}, \frac{1}{4}, \frac{1}{4})$ from the structure in Fig. 1(a).

have performed a cluster simulation based on the crystal structure of cubic C_3 phase.³² The average value for the cubic cell dimension is estimated to be 5.48 and 5.57 Å by LDA and GGA, respectively. This suggests a notable $\sim 3\%$ expansion in the lattice parameter value of the nanocrystal from our calculated equilibrium bulk lattice parameters, and offer insights for understanding the variation of experimental data.^{16,17}

Figure 1(f) shows the calculated band structure of cubic C_3 carbon using the hybrid functionals (HSE06) under LDA.²³ The valence band top is at the X point and the conduction band bottom is at the Γ point; The calculated band gap is 3.05 eV, which is considerably smaller than the gap of 5.43 eV for diamond. Therefore, cubic C_3 carbon is an indirect band-gap semiconductor.

Since energetic calculations alone cannot establish the stability of a crystal structure,³³ to confirm further the mechanical stability of C_3 carbon, we have also calculated its phonon dispersion curves within a wide pressure range up to 160 GPa (see Fig. 2). No imaginary frequencies were observed throughout the entire Brillouin zone

implying the kinetical stability of C_3 carbon.

We now address the critical issue of atomistic mechanism underlying the transformation from graphite toward cubic C_3 carbon. The kinetic processes at the atomic scale are simulated using the climbing image nudged elastic band (CI NEB) method³⁴ with a 24-atom supercell containing two carbon sheets in AB stacking. No symmetry constraint was imposed in the structural optimization procedure. In contrast to the c -axis compression process from graphite to M or W carbon,¹⁴ we here identify a strong in-plane anisotropic compression pathway along $a[100]$ axis. In Fig. 3(a), a rectangular supercell in $P6_3/mmc$ (no.194) symmetry is used to simulated the initial graphite with lattice parameters $(x, y, z) = (7.333 \text{ \AA}, 4.239 \text{ \AA}, 6.567 \text{ \AA})$, where x and y axes are parallel to the $a[100]$ and $b[210]$ directions of graphite, respectively. Under the compression, the graphitic sheets are first rumpled with a wave-like structural pattern [Fig. 3(b)], which is driven by an in-plane anisotropic compression along the $a[100]$ direction. Meanwhile, the adjacent carbon sheets slip to each other along the $b[210]$

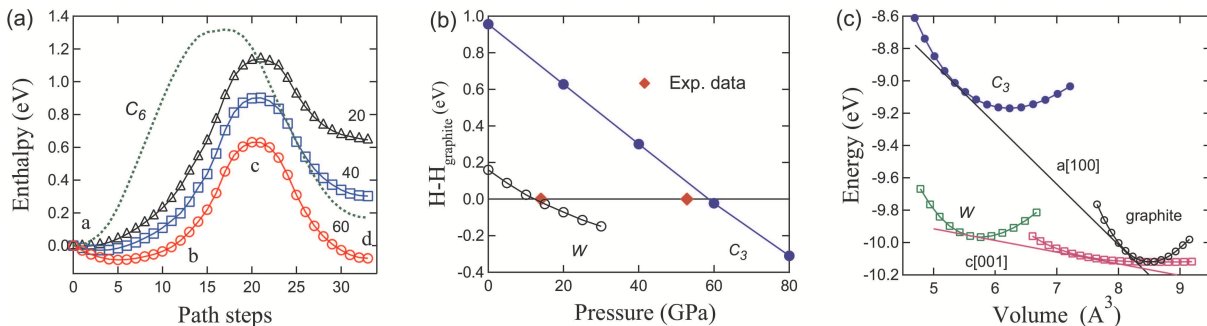


FIG. 4: (color online). (a) Enthalpy versus transformation pathway step for graphite-to- C_3 transition at 20, 40 and 60 GPa. The letters "a," "b," "c," and "d" refer to the images in the respective panels in Fig. 3. The dot line represents the enthalpy for graphite-to- C_6 transition at 60 GPa. (b) The enthalpy per atom for cubic C_3 carbon and W carbon¹⁴ as a function of pressure relative to graphite. The experimental transition points¹⁶ are indicated. (c) Total energy as a function of volume for cubic C_3 carbon and W carbon, in comparison with those for graphite under anisotropic $a[100]$ or $c[001]$ compression. The common tangents for calculating the transition pressures are shown.

direction. It is followed by further distortion of the rumpled carbon sheets to form benzene rings along the in-plane diagonal direction [Fig. 3(c)], which is caused by anisotropic lattice expansion along the $b[210]$ direction and large compressive stress along the $a[100]$ direction. At the same time, a local rotation and distortion of the benzene rings take place, which promotes cross-linking of the benzene rings between adjacent graphite sheets, driving the system toward the new cubic C_3 carbon phase. In Fig. 3(d), four zigzag C_6 rings are linked in a diamond topology, located at $(\frac{1}{4}, \frac{1}{4}, \frac{1}{4})$, $(\frac{3}{4}, \frac{3}{4}, \frac{1}{4})$, $(\frac{1}{4}, \frac{3}{4}, \frac{3}{4})$ and $(\frac{3}{4}, \frac{1}{4}, \frac{3}{4})$ position, and the C_6 rings contact to each other to form eight trigonal C_3 rings as shown in Fig. 1(a). Throughout the transformation pathway, the structures from step 1 to 17 are in $Pbcn$ (no.60) symmetry and the structures from step 18 to 32 are in $Pbca$ (no.61) symmetry (e.g., b and c in Fig. 3) remain in high symmetry, resulting in a smooth conversion process.

Figure 4(a) shows the enthalpy along the pathway toward the formation of cubic C_3 carbon under pressure at 20, 40, and 60 GPa. It is shown that graphite's layered structure makes the rumpling of the the graphitic sheets relatively easy to occur at the early stages of structural transformation under compression. With the local rotation of the benzene rings, the enthalpy increases quickly due to bond twisting and breaking; and then the enthalpy decreases with the cross linking of the benzene rings between adjacent layers. Pressure plays a key role in lowering the kinetic barrier and facilitates the phase transformation. For comparison, we also considered the graphite-to- C_6 transition at 60 GPa. However, it is clearly unfavorable by both kinetics and energetics [see Fig. 4(a)]. These results suggest an effective route for the synthesis of cubic C_3 carbon under high pressure.³⁵

It should be noted that there are two distinct phase transformations observed in the experiment¹⁶ as indicated in Fig. 4(b). The first occurs at a relatively low pressure of 13~15 GPa, which corresponds to the formation of Z carbon³⁶ and W carbon¹⁴ [results for W

carbon shown in Fig. 4(b)], and it is characterized by a marked increase in electrical resistivity;⁷⁻¹⁰ however, this compressed phase reverts to graphite with the release of pressure at room temperature. A second phase conversion is observed at much higher pressure above 50 GPa, which corresponds to the formation of the new cubic carbon phase¹⁶ [see Fig. 4(b)]. To clarify this point, we have calculated the total energy as a function of volume for cubic C_3 , W carbon and for graphite under anisotropic $a[100]$ or $c[001]$ compression [see Fig. 4(c)]. Using the relation $P = -\frac{\Delta E}{\Delta V}$ and the common tangent of the total energy curves in Fig. 4(c), the critical pressures are estimated to be 11.3 GPa for the graphite-to- W carbon transition along the $c[001]$ compression and 59.0 GPa for the graphite-to- C_3 carbon transition along the $a[100]$ compression. The calculated values are in good agreement with the corresponding experimental data [see Fig. 4(b)], indicating that our computation has captured the main physics. These results establish a new anisotropic compression synthesis process to form cubic C_3 phase, which is distinct from the usual c -axis compression for the graphite-to-diamond phase transformation.¹⁻¹⁵

In summary, we have resolved the long-standing problem of structural identification of a new cubic carbon phase that consist of a three-dimensional sp^3 -connected network of trigonal C_3 rings in $Pa\bar{3}$ (T_h^6) symmetry, and unveiled a graphitic sheet-rumpling mechanism for the phase transition. It suggests an anisotropic graphite a -axis compression synthesis route for cubic C_3 carbon, which is distinct from the c -axis compression for the graphite-to-diamond transition. This new mechanism may also provide insights for understanding structural transformation in other covalent materials, such as cubic $[B_{12}N_{12}]$ -FAU zeolite,³⁷ that convert from starting materials of layered structure.

This study was supported by the NSFC of China (Grant No. 10974230) and the Ministry of environmental protection of China (Grant No. 200909086, 201109037). C.F.C acknowledges support by DOE under Cooperative

Agreement DE-FC52-06NA27684. Acknowledgment goes to the CREST project headed by Professor M. Kotani for the support. We are thankful to the crew of the Cen-

ter for Computational Materials Science at IMR, Tohoku University for their support at the SR11000 supercomputing facilities.

-
- * e-mail address:wjt@aphy.iphy.ac.cn
- ¹ F. P. Bundy and J. S. Kasper, *J. Chem. Phys.* **46**, 3437 (1967).
 - ² R. Clarke and C. Uher, *Adv. Phys.* **33**, 469 (1984).
 - ³ T. Irifune, A. Kurio, S. Sakamoto, T. Inoue, and H. Sumiya, *Nature (London)* **421**, 599 (2003).
 - ⁴ H. Sumiya and T. , *J. Mater. Res.* **22**, 2345 (2007).
 - ⁵ F. P. Bundy, W. A. Bassett, M. S. Weathers, R. J. Hemley, H. K. Mao, and A. F. Goncharov, *Carbon* **34**, 141 (1996).
 - ⁶ E. D. Miller, D. C. Nesting, and J. V. Badding, *Chem. Mater.* **9**, 18 (1997).
 - ⁷ W. Utsumi and T. Yagi, *Science* **252**, 1542 (1991).
 - ⁸ M. Hanfland, K. Syassen, and R. Sonnenschein, *Phys. Rev. B* **40**, 1951 (1989).
 - ⁹ T. Yagi, W. Utsumi, M. A. Yamakata, T. Kikegawa, and O. Shimomura, *Phys. Rev. B* **46**, 6031 (1992).
 - ¹⁰ Y. X. Zhao and I. L. Spain, *Phys. Rev. B* **40**, 993 (1989).
 - ¹¹ W. L. Mao, H. K. Mao, P. J. Eng, T. P. Trainor, M. Newville, C. C. Kao, D. L. Heinz, J. F. Shu, Y. Meng, and R. J. Hemley, *Science* **302**, 425 (2003).
 - ¹² M. Hanfland, H. Beister, and K. Syassen, *Phys. Rev. B* **39**, 12598 (1989).
 - ¹³ Q. Li, Y. M. Ma, A. R. Oganov, H. B. Wang, H. Wang, Y. Xu, T. Cui, H. K. Mao, and G. T. Zou, *Phys. Rev. Lett.* **102**, 175506 (2009).
 - ¹⁴ J. T. Wang, C. F. Chen, and Y. Kawazoe, *Phys. Rev. Lett.* **106**, 075501 (2011).
 - ¹⁵ J. T. Wang, C. F. Chen, and Y. Kawazoe, *Phys. Rev. B* **84**, 012102 (2011).
 - ¹⁶ R. B. Aust and H. G. Drickamer, *Science* **140**, 817 (1963).
 - ¹⁷ M. Miki-Yoshida, L. Rendon, and M. Jose-Yacamán, *Carbon* **31**, 843 (1993).
 - ¹⁸ J. M. Cowley, R. C. Mani, M. K. Sunkara, M. O’Keeffe, and C. Bonneau, *Chem. Mater.* **16**, 4905 (2004).
 - ¹⁹ G. Kresse and J. Furthmüller, *Phys. Rev. B* **54**, 11169 (1996); G. Kresse and J. Hafner, *ibid.* **47**, 558 (1993).
 - ²⁰ D. M. Ceperley and B. J. Alder, *Phys. Rev. Lett.* **45**, 566 (1980); J. P. Perdew and A. Zunger, *Phys. Rev. B* **23**, 5048 (1981).
 - ²¹ J. P. Perdew, K. Burke, and M. Ernzerhof, *Phys. Rev. Lett.* **77**, 3865 (1996).
 - ²² P. E. Blöchl, *Phys. Rev. B* **50**, 17953 (1994); G. Kresse and D. Joubert, *Phys. Rev. B* **59**, 1758 (1999).
 - ²³ A. V. Krukau, O. A. Vydrov, A. F. Izmaylov, and G. E. Scuseria, *J. Chem. Phys.* **125**, 224106 (2006).
 - ²⁴ K. Parlinski, Z.-Q. Li, and Y. Kawazoe, *Phys. Rev. Lett.* **78**, 4063 (1997).
 - ²⁵ H. Terrones and A. L. Mackay, *Carbon* **30**, 1251 (1992).
 - ²⁶ V. L. Bekenev and V. V. Pokropivny, *Phys. Solid State* **48**, 1405 (2006).
 - ²⁷ F. Jensen and H. Toftlund, *Chem. Phys. Lett.* **201**, 89 (1993).
 - ²⁸ J. Gibson, M. Holohan, and H. L. Riley, *J. Chem. Soc.* **456** (1946).
 - ²⁹ M. O’Keeffe, G. B. Adams, and O. F. Sankey, *Phys. Rev. Lett.* **68**, 2325 (1992).
 - ³⁰ F. Occelli, P. Loubeyre, and R. Letoullec, *Nature Mater.* **2**, 151 (2003).
 - ³¹ Besides the C_3 , C_4 and C_6 carbon, there is another P -type cubic carbon in $Pm\bar{3}$ (no. 200) symmetry occupying the 24j (0.25, 0.3597, 0.1403) position, which is a zero-gap semiconductor. However, it is highly unstable in energy and omitted here.
 - ³² A super cell $36 \text{ \AA} \times 36 \text{ \AA} \times 36 \text{ \AA}$ with 1536 carbon atoms and a Γ point in the Brillouin zone are used.
 - ³³ Y. Yao, J. S. Tse, J. Sun, D. D. Klug, R. Martonak, and T. Iitaka, *Phys. Rev. Lett.* **102**, 229601 (2009).
 - ³⁴ See [<http://theory.cm.utexas.edu/henkelman>] for study of the kinetic processes at the atomic scale.
 - ³⁵ To understand the thermodynamic stability of the C_3 phase, we have also investigated the phase conversion from C_3 to an I-24 phase in $Ia\bar{3}d$ (no. 230) symmetry. We find that the C_3 phase can smoothly convert to I-24 phase and maintain the $Pa\bar{3}$ (no. 205) symmetry throughout the transformation pathway; but it encounters a relatively larger barrier of 0.93-0.96 eV under a wide pressure range of 0~60 GPa. These results indicate high stability of C_3 phase in energetics and kinetics at room temperature.
 - ³⁶ M. Amsler, J. A. Flores-Livas, L. Lehtovaara, F. Balima, S. A. Ghasemi, D. Machon, S. Pailhes, A. Willand, D. Caliste, S. Botti, A. SanMiguel, S. Goedecker, and M. A. L. Marques, *Phys. Rev. Lett.* **108**, 065501 (2012).
 - ³⁷ A. V. Pokropivny, *Diamond Relat. Mater.* **15**, 1492 (2006).